On the formation of gamma-coherent cell assemblies by oriens lacunosum-moleculare interneurons in the hippocampus

Adriano B. L. Tort*†‡, Horacio G. Rotstein§, Tamar Dugladze¶, Tengis Gloveli¶, and Nancy J. Kopell*‡

*Department of Mathematics and Center for Biodynamics, Boston University, Boston, MA 02215; †Departamento de Bioquímica, Instituto de Ciências Básicas da Saúde, Universidade Federal do Rio Grande do Sul, RS 90035-003, Porto Alegre, Brazil; §Department of Mathematical Sciences, New Jersey Institute of Technology, Newark, NJ 07102; and ¶Institute of Neurophysiology, Charité-Universitätsmedizin Berlin, 10117 Berlin, Germany

Gamma frequency (30–80 Hz) network oscillations have been observed in the hippocampus during several behavioral paradigms in which they are often modulated by a theta frequency (4–12 Hz) oscillation. Interneurons of the hippocampus have been shown to be crucially involved in rhythms generation, and several subtypes with distinct anatomy and physiology have been described. In particular, the oriens lacunosum-moleculare (O-LM) interneurons were shown to synapse on distal apical dendrites of pyramidal cells and to spike preferentially at theta frequency, even in the presence of gamma-field oscillations. O-LM cells have also recently been shown to present higher axonal ramification in the longitudinal axis of the hippocampus. By using a hippocampal network model composed of pyramidal cells and two types of interneurons (O-LM and basket cells), we show here that the O-LM interneurons lead to gamma coherence between anatomically distinct cell modules. We thus propose that this could be a mechanism for coupling longitudinally distant cells excited by entorhinal cortex inputs into gamma-coherent assemblies.

oscillations | coherence | synchrony | theta rhythm

Fig. 1. O-LM cells posses higher axonal projections in the longitudinal direction of the CA3 area. Neurolucida reconstructed biocytin-filled O-LM cell in area CA3 from transverse (*Left*) and longitudinal slices (*Right*). The soma and dendrites are drawn in red, whereas the axon is in green. The horizontal dendritic branches were restricted to the stratum oriens. The axons crossed the pyramidal cell layer and extensively innervated the stratum lacunosum-moleculare of the area CA3. Note the much longer axonal ramification pattern in stratum lacunosum-moleculare of the longitudinal slice than of the transverse slice. Hippocampal layers are depicted schematically. CA3, CA3 area; str. or., stratum oriens; str. pyr., stratum pyramidale; str. rad., stratum radiatum; str. l.-m., stratum lacunosum-moleculare.

Oscillations in cortical structures have been observed in many species (1–3), and among them gamma oscillations (30–80 Hz) have received special attention because of their supposed role in complex functions as sensory binding (2, 3), attention selection (4, 5), and conscious experience (6, 7). Gamma oscillations are prominent in the hippocampus and entorhinal cortex (EC), frequently nested within a theta rhythm (4–12 Hz), and they are thought to be involved in transient neuronal assembly formation (8, 9) and information transmission and storage (10–12). There is compelling evidence that hippocampal interneurons have a pivotal role in driving gamma- and theta-frequency network oscillations (13–20).

GABAergic interneurons present a large morphological and functional heterogeneity in the hippocampal subfields (20–22). Inhibitory interneurons that control the firing of principal cells include the perisomatic-targeting interneurons (e.g., fast-spiking basket cells) and dendritic-targeting interneurons (20–22). Oriens lacunosum-moleculare (O-LM) interneurons belong to the latter group and are characterized by the cell body and dendritic trees lying horizontally in the stratum oriens, whereas the axon innervates the stratum lacunosum-moleculare (23). The outputs of these cells are projected as slow inhibitory postsynaptic potentials (IPSPs) onto the distal apical dendrites of pyramidal neurons (24). Recently, it was shown that in the CA3 region O-LM interneurons arborize most extensively in the longitudinal axis of the hippocampus (18).

Gamma oscillations in the hippocampus can be modulated by theta frequency rhythms both *in vivo* (25–27) as well as in *in vitro* (28). This phenomenon may reflect a division of function among interneurons, with the two frequencies generated by distinct subclasses of interneurons. During the gamma rhythm, Gloveli *et al.* (19) reported that O-LM cells fire at theta frequencies (every 4–5 gamm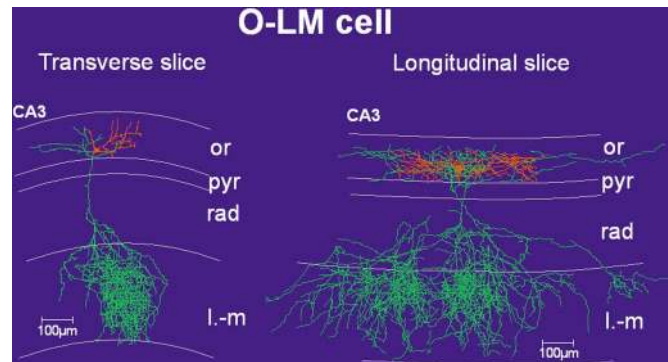a periods), whereas basket cells tend to fire at each gamma period. In the present work, we use a biophysical hippocampal network model to show that O-LM cells are able to create gamma-coherent cell assemblies among subsets of distant CA3 transversal cell modules.

Results

O-LM Cells Present Higher Axonal Projections in the Longitudinal Axis of the Hippocampus. Biocytin-labeled O-LM interneurons displayed a previously described horizontal organization of dendritic tree and axonal termination in the stratum oriens and lacunosum-moleculare (Fig. 1). These cells arborized most extensively in the longitudinal plane (the maximal axonal spread was 1,300 μm and 1,200 μm in two cells) than in the transverse direction (223.7 $\pm$ 12.2 μm, $n = 6$). This result confirmed our previous findings and, moreover, showed that the longitudinal projection of CA3 O-LM cells is wider than that of CA1 O-LM neurons described in ref. 29.
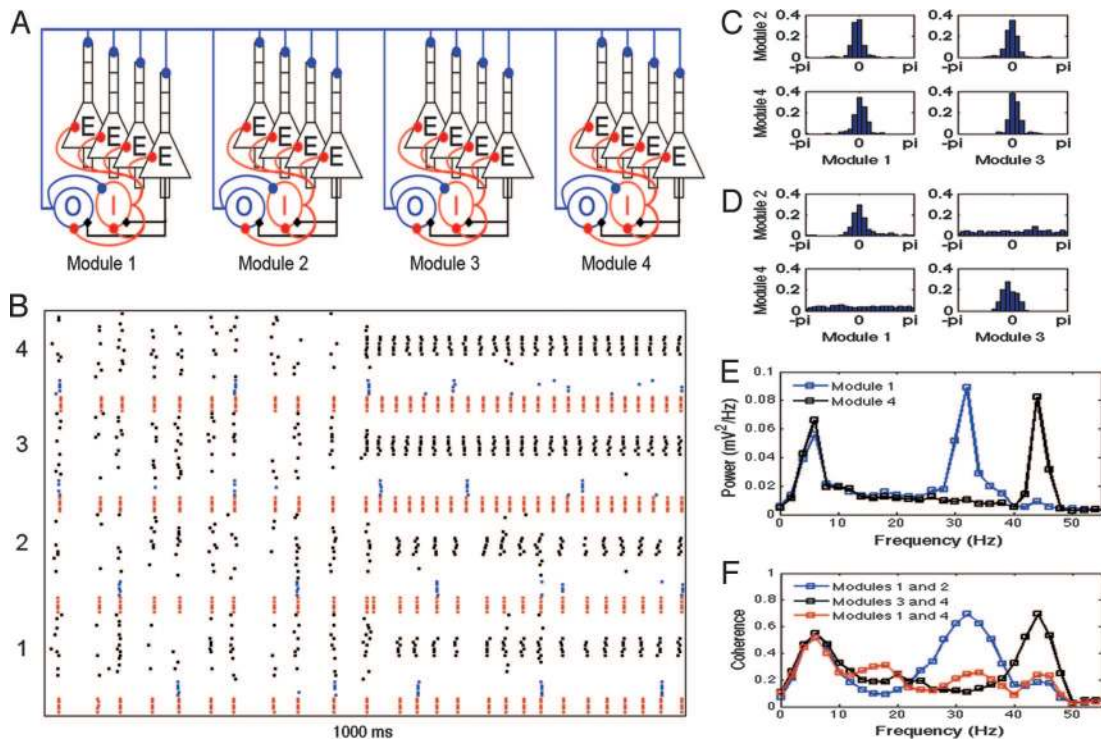
Fig. 2. O-LM cells coordinate multiple cell assemblies. (*A*) Network scheme. Within each module, O-LM (O) cell population inhibits the distal apical dendrites of pyramidal (E) cell population, basket (I) cell population inhibits E cell at the soma and also inhibits itself and O cell population, and E cell excites both O and I cells. Connections among modules are made through O–E synapses on distal apical dendrites. (*B*) Representative spike rastergram of a network consisting of four modules (labeled 1 to 4 on the *y* axis). Each module consisted of 40 E (black), 10 O (blue), and 10 I cells (red). For clarity, however, just half the number of cells is shown. During the first 500 ms, all E cells received drive currents uniformly distributed from 217–236 pA. Note that E cells spike sparsely and randomly (6.72 ± 2.76 Hz) in this regime and that O–E synapses are able to induce synchrony among modules. For the second 500 ms of simulation, 12 E cells inside each module were activated with higher drive currents. E cells of modules 1 and 2 received random drive from 330–349 pA, whereas activated E cells in modules 3 and 4 received drive from 820–849 pA. Note the suppression of the less active E cells inside each module as well as the formation of two distinct gamma assemblies induced by O–E synapses. (*C*) Normalized phase difference histograms obtained for the parameter regime shown in the first 500 ms of *B*, showing synchrony among all modules. (*D*) Same as in *C*, but for the regime shown in the second 500 ms of *B*. Note the loss of synchrony between modules with distinct levels of excitation. (*E*) Power spectra of the model LFPs of modules 1 and 4 after the activation of subsets of E cells showing theta and (distinct) gamma peaks. (*F*) Coherence analysis between modules of similar and distinct activated E cell drives. Note the loss of gamma coherence between modules of distinct drive along with no change in theta coherence. *C–F* were obtained by analyzing 10 s of simulation. E cell drive was applied at the distal apical dendritic compartment. Other parameters are presented in SI Table 1. The same color convention for the cells will be used in the other rastergrams.

The present data were obtained from the mouse hippocampus, which is significantly smaller than the rat hippocampus. We note that the mechanisms of rhythms generations in the mouse and in the rat hippocampus have been described as similar (30).

O-LM Cells Can Coordinate Multiple Cell Assemblies. In Fig. 2 we show the results obtained for a network composed of four modules, which was simulated under two regimes: (*i*) with the E cells of each module spiking sparsely and randomly and (*ii*) after exciting a subset of E cells inside each module (see the Fig. 2 legend). We observed that O–E synapses are able to make modules synchronize in both regimes. We also found that O–E connections allow the coexistence of multiple gamma-cell assemblies (each assembly being formed by subsets of cells having similar drive/frequency) as well as the coexistence of active cell assemblies and nonexcited modules (Figs. 2 and 3*C*).

Gamma Oscillations Are Nested in Theta Frequency Oscillations in Simple Module Networks. Due to computational time constraints and for clarity of understanding, further detailed characterization of the O–E-induced gamma synchrony reported here was performed in networks composed of simple modules. The module synchronization phenomena we demonstrate do not require more than one E cell per module; the more complicated simulations of Fig. 2 show that the cell assembly phenomena still exists even when

the E cells in each module are not synchronous. In Fig. 3*A* we show the most common dynamics of such networks. Note that O–E synapses are able to induce gamma synchrony between modules in these simpler networks; again, these connections permit the coexistence of multiple gamma frequencies in this type of network (Fig. 3*C*). Within each module, the E and I cells interact with each other, generating a pyramidal–interneuronal gamma (PING) rhythm in this subnetwork (see ref. 5 for a short review), whereas O cells tend to fire in clusters at theta frequency. The local field potential (LFP) exhibits a mixed rhythm, which is more evident in the apical dendrites, and the theta power magnitude diminishes from the distal apical dendrites to the soma. Similar results were obtained in a network composed of just one simple module [see supporting information (SI) Fig. 6]; this behavior was very robust to change in parameters, and it was not dependent on the number of each interneuron cell type in the network (data not shown).

Theta Rhythm Is Not Necessary for O–E-Induced Gamma Synchrony. When working with simple module networks, we often observed the O cells firing in clusters at theta frequency within a module, and, moreover, these theta clusters were commonly synchronous among modules (Fig. 3*A* and SI Figs. 6 and 7). However, this latter result was not universal, and we also observed gamma synchrony without theta synchrony among modules. More rarely, there were also cases in which the O cells fired asynchronously
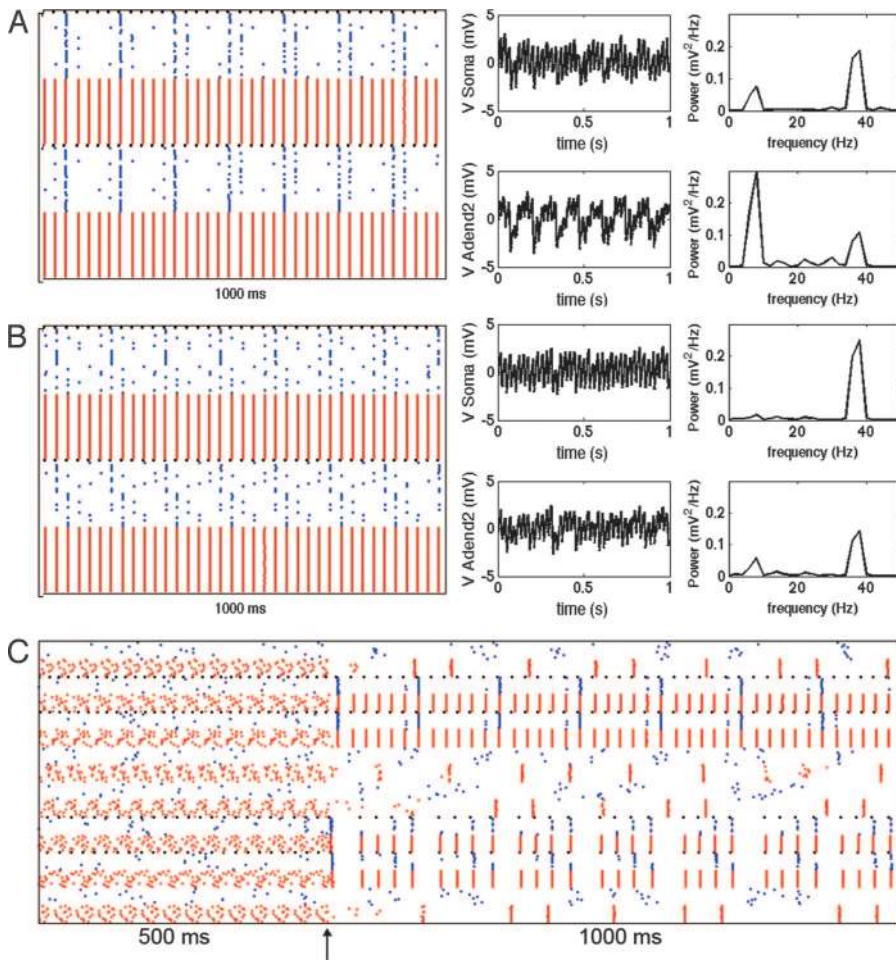
Fig. 3. O–E synapses lead to gamma synchrony between modules even when the O cells spike asynchronously. (*A*) Representative spike rastergram (*Left*) of two connected modules (1 E, 25 O, and 25 I cells each). Model LFPs of the bottom module (*Center*; at Soma and Adend2 compartments; see *SI Appendix*) and the corresponding power spectrum analysis (*Right*) are shown. These graphs represent the most common behavior of this network: E and I cells of both modules spike synchronously at gamma frequency and the O cells tend to spike at theta clusters, which are often synchronous between modules (G_{OE} between modules = 8 mS). (*B*) Same as in *A*, showing, however, a case in which the O cells do not display clear spikes at theta clusters (especially in the *Lower* module). Note the reduction of the peak theta power compared with the case shown in *A*. However, even in these cases of O cell asynchrony, O–E synapses always lead to gamma synchrony between modules. (*C*) Representative rastergrams of a network composed of eight modules (1 E, 15 I, and 15 O cells each). O–E synapses allow the coexistence of synchronization of two modules of high drive (848 pA; the two excited *Upper* modules) and of two modules of low drive (424 pA; the two excited *Lower* modules), whereas four nonexcited modules remain asynchronous (G_{OE} among modules = 5 mS). The arrow indicates the time synapses were turned on. Note that in this example both gamma assemblies present the same theta rhythm. Other parameters are presented in SI Table 2.

within a module, with the corresponding model LFP exhibiting a great decrease or even disappearance of the theta peak. Even in these cases, however, O–E synapses always induced gamma synchrony among modules (see Fig. 3*B*).

O–E Connections Induce Gamma Synchrony Even in the Presence of Conduction Delays and Low Synaptic Strength. The O–E-induced gamma synchrony was robust to a wide range of changes in parameters (see further results) and also to conduction delay times for O–E synapses between modules up to 8–9 ms (Fig. 4*B* and SI Fig. 7). Moreover, even values of O–E conductance (G_{OE}) between modules as low as 35% (compared with the value of this conductance within a module) were able to synchronize the modules at gamma frequency (Fig. 4*A* and SI Fig. 7). Increasing the number of modules in the network makes this G_{OE} cutoff percentage even smaller (see SI Fig. 7; note, however, that this conductance is only normalized by the number of O cells inside a module and not by the number of modules in the network).

O–E-Induced Gamma Synchrony Persists with Weighted Delay and Weighted Synaptic Strength. O–E connections are still able to induce gamma synchrony in a network composed of 10 modules when conduction delays and synaptic strength are weighted among modules by length between modules. By studying networks with restricted O–E axonal projections among modules (i.e., non-all-to-all O–E connections among modules), we observed both cases of gamma synchrony between nondirectly connected modules, as well as cases of formation of distinct assemblies with the same gamma frequency, depending on whether there existed a polysynaptic path

among the excited modules. Details about these sets of simulations and the corresponding results can be found in SI Fig. 8.

PING Is Required for O–E-Induced Gamma Synchrony Among Modules. By changing the drive to the pyramidal cell population (Fig. 5), we observed that synchrony among modules is only possible when both modules are exhibiting a PING rhythm, i.e., a minimal level of E drive is required for gamma synchrony, and this level coincides with the value at which the E cell frequency reaches the I cell frequency (Fig. 5*B*). Qualitatively similar results were obtained for several changes in the values of parameters, including the level of white noise, delay time, and O–E conductance between modules (data not shown). Note that Fig. 5*B* also shows that the frequencies of gamma (I cell) and theta (O cell) covary as the level of E drive is increased.

Mutual Inhibition Among Basket Cells Is Necessary for Robustness of O–E-Induced Gamma Synchrony. We found that a minimal level of I–I conductance (G_{II}) is necessary for synchronization between modules using the current parameters values (see SI Fig. 9). Without this synapse, I cells spike at a very high frequency driven by E cell excitation. However, if G_{II} is too high, the I cells start firing at a lower frequency than the E cells. At this point, PING is broken, and gamma synchrony between modules is lost (SI Fig. 9). By increasing the strength of E–I synapses, PING and gamma synchrony between modules are restored (data not shown). By lowering the strength of E–I synapses, we found that O–E synapses are able to induce gamma synchrony in the absence of I–I connections but only in a very small range of parameter values and not for all initial conditions (data not shown).
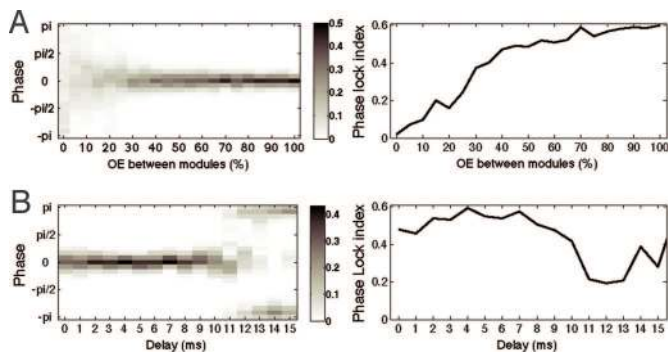
Fig. 4. Influence of delay and synaptic strength on O–E-induced gamma synchrony. (*A*) (*Left*) Color histograms of gamma phase difference of two modules for distinct values of G_{OE} between modules (expressed as percent of G_{OE} within a module). (*Right*) Values for the corresponding phase lock index (PLI). (*B*) Gamma synchrony induced by O–E synapses between two modules persists with delay values compatible with the anatomy. (*Left*) Color histograms of gamma phase difference between two modules are plotted for distinct delay times (G_{OE} between modules = 60% of G_{OE} within). (*Right*) Values for the corresponding PLI. Note the tendency of antiphase for delay times near half gamma period. For all these simulations, each module was composed of one E, five O, and five I cells. Other parameters values are the same as in Fig. 3.

Distinct Levels of Pyramidal Cell Drive or Intramodule Mutual Inhibition Lead to Gamma Phase-Locking with Nonzero Lag. Network of modules presenting distinct levels of pyramidal cell drive can create a nonzero phase-lag (SI Fig. 10). We observed that, in comparison with a module of fixed E drive, lower E drive leads to gamma phase-delay, whereas higher E drive leads to gamma phase-advance (SI Fig. 10). We also observed that lower G_{II} values lead to gamma phase-advance, and higher values lead to gamma phase-delay in relation to a module with fixed G_{II} (SI Fig. 11). Note, however, that if G_{II} inside one module is high enough, PING in this module is broken, and gamma synchrony between modules is lost (SI Fig. 11), in agreement with the results presented above.

Distal Apical Dendrite Location of O–E Synapses and Drive Current Produces More Robust Gamma Synchrony/Phase-Locking Among Modules Than the Somatic Location of Both Drive and Synapses. To understand whether the distal location of EC inputs and O-LM synapses are important, we modified the network architecture by changing both E drive and O–E synapse locations to the soma compartment and compared the network behavior with the usual network architecture. Gamma synchrony between modules induced by the distal location of inputs was much more robust than the somatic location, because it persisted with levels of G_{OE} between modules as low as 35% compared with 70% for the somatic location (see SI Fig. 12). The same qualitative results were obtained for other baseline E drives, delay times, white noise level, and number of modules in the network (data not shown). We also found that the gamma synchrony/phase-locking induced by the distal location of O–E synapse and E drive tolerates much bigger drive differences between modules than the somatic location (see SI Fig. 10). Depending on the network parameters, E drive percentage difference between two modules leading to gamma phase-locking is usually 12–20%, compared with 2–6% for the soma mode.

Discussion

Motivated by recent experimental findings (16, 18, 19), we have constructed a biophysical CA3 model network taking into account the anatomical and physiological properties of the O-LM interneuron. The results presented here are in agreement with experimental findings showing coexistence of gamma and theta rhythms in the hippocampus. The main result suggested by our computational model is that O-LM interneurons are able to bring about gamma synchrony among cells within transverse CA3 modules located anatomically distant along the longitudinal axis of the hippocampus. These cells could thus be involved in the formation of dynamic CA3 cell assemblies associated with EC excitatory inputs. Indeed, the synchrony could provide a substrate for Hebbian or heterosynaptic plasticity for later recall.

It is known that the theta rhythm is coherent over larger distances than the gamma rhythm (ref. 31, but see also ref. 25). The use of the theta-producing O-LM cells to create cell assemblies temporally organized at the gamma rhythm raises the question of whether this is compatible with the more local coherence of gamma. We note that CA3 is known to produce gamma as an interaction of pyramidal cells and proximal basket cells (27); this rhythm is likely to be the major contributor to the measured gamma rhythm. Thus, the latter may be only locally coherent, although there could exist cell assemblies including subsets of pyramidal cells more globally dispersed along the longitudinal axis.

The O–E-induced gamma synchrony tolerates high values of delay time (up to 8–9 ms; Fig. 4B). The mechanism here may be related to a previous mechanism for gamma synchrony over a long distance by using timing of basket cell doublets (32). In the current case, the pyramidal cells receive inhibition from both local O-LM cells and the O-LM cells of at least one other module; this gives rise to a pair of inhibitory postsynaptic potentials (IPSPs) in the pyramidal cells whose relative timing may play the same role as the relative timing of the inhibitory doublets. We have found that the synchronization does not require the long IPSPs of O-LM cells, nor special currents in either the pyramidal or O-LM cells (data not shown). However, it does require that the pyramidal cell population fires at gamma frequencies; the synchronization breaks down when the pyramidal cells fire too slowly. Thus, the mechanism is not the same as that in ref. 15 in which long-range inhibition produces synchrony in a completely inhibitory network. Also, the synchrony in the current work is not produced just from common inhibition because, in the presence of graded delays, different pyramidal cells receive inhibition at different times.

In our model, the E/I subnetwork generates the gamma rhythm inside each cell module, whereas the E cells also drive the O cells to generate the theta rhythm. Because the pyramidal cells provide both interneuron types with excitatory inputs, both theta and gamma frequencies change together; note that the ratio of the frequencies remains roughly constant (Fig. 5B), in agreement with experimental results (25). Our results showed that an excitation-dependent gamma (PING) inside modules is necessary for the formation of cell assemblies, i.e., the pyramidal cells as a population should fire at a frequency no less than the basket cells (Fig. 5 and SI Figs. 9 and 11), and, moreover, they should drive these cells. This phenomenon requires a minimal excitatory drive to pyramidal cells for the formation of cell assemblies, which could be due to direct excitation by the EC and/or pyramidal cell mutual excitation. We observed that the higher the I_h conductance (or the positive shift in its activation curve) the higher the E cell frequency (data not shown). Hence, activation of this current could also be a mechanism leading to PING generation and subsequent formation of cell assemblies.

We often observed that the O-LM cells within a module (and also among modules) tend to fire in clusters at theta frequency (Fig. 3A and SI Figs. 6 and 7), in agreement with previous work *in vitro* showing the existence of an intrahippocampal mechanism of theta generation (16, 18, 19, 28). The O-LM cells were still able to lead to gamma synchrony among modules even for the cases in which they were not firing in clusters within a module and also when the clusters were asynchronous among modules (see Fig. 3B). Thus, O-LM interneurons could lead to higher gamma coherence among cell modules even in the absence of a perceptible theta rhythm in the field potential.
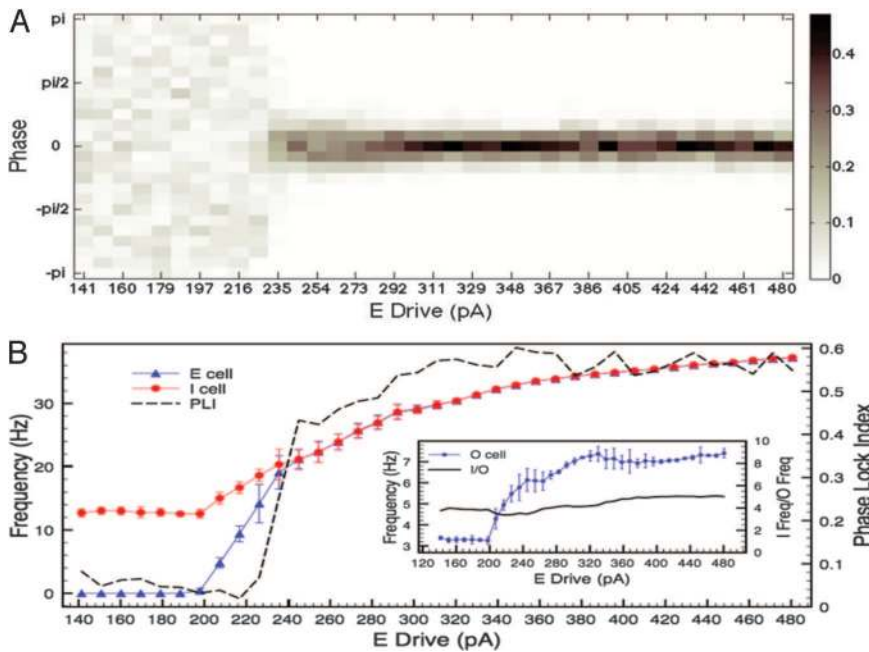
NEUROSCIENCE

Fig. 5. PING is required for O–E induced gamma synchrony between modules. (*A*) Color histograms of gamma phase difference between two connected modules for distinct values of E cell drive. Note that a minimal level of E drive is required for synchrony. (*B*) Plots of E and I cells frequencies (left vertical scale) and the phase lock index (PLI) (right vertical scale) for distinct values of E cell drive. (*Inset*) O cell frequency (left vertical scale) and the ratio of I cell frequency to O cell frequency (right vertical scale) as a function of E cell drive. Note that gamma synchrony between modules emerges when E cell frequency reaches I cells frequency, which is when the E/I subnetwork starts exhibiting PING. Notice also that both gamma (I cell) and theta (O cell) frequencies covary with E drive. Error bars represent SD. Each module consisted of one E, five I, and five O cells. Other parameters values are the same as in Fig. 3.

We observed two situations in which gamma phase-advance or -delay occurred between a module and another taken as the reference gamma rhythm: we showed that distinct E drive as well as distinct level of mutual I–I inhibition could lead to gamma phase-locking with nonzero lags (SI Figs. 10 and 11). These two cases probably share a common mechanism, because increasing I–I conductance inside a module diminishes its network gamma frequency and vice versa, as is the case for less and more levels of E drive respectively. Thus, the nonzero phase lags are probably a reflection of the generic property of paired oscillators that the faster oscillator leads the slower one (33).

On the basis of known anatomy, we worked mainly with the E drive (and O–E synapses) located at the distal apical dendrites of pyramidal cells, intended to represent the EC input into the CA3 region. We found that this configuration was more robust in leading to assembly formation than when both the E drive and the O–E synapses were located at the soma (SI Figs. 10 and 12): we showed that the gamma phase-locking induced by distal inputs tolerates much bigger E drive differences between modules than that induced by somatic inputs (SI Fig. 10). This result probably reflects the differences in the $f - I_{app}$ curves associated with these compartments and may thus be related to distinct synaptic integration properties of the dendritic tree and the soma. Our results suggested that I_A has an important role in making the dendritic $f - I_{app}$ curve flatter than the somatic $f - I_{app}$ curve (data not shown), in agreement with previous studies reporting the role of this current in controlling dendritic excitability (34). We also found that the gamma phase-locking induced by the somatic inputs is much more sensitive to low levels of O–E synaptic conductances between modules than the locking induced by distal inputs (SI Fig. 12).

The network architecture used here is general enough to represent other hippocampal regions, notably the dentate. Sik *et al.* (35) described hilar interneurons densely innervating the outer molecular layer, i.e., with perforant pathway-associated axon terminals (HlPP cells). Because these cells also presented large septo-temporal projections (35), we postulate that they could serve the same function in the dentate as O-LM cells in CA3. Noteworthy, Bragin *et al.* (25) described high levels of gamma coherence along the longitudinal axis of the hilar region *in vivo*. In the CA1 region, dendritic targeting interneurons with

longer longitudinal projections have yet to be described. Long-range GABAergic cells synapsing on interneurons have been described in the hippocampus, and they most likely are also involved in bringing higher rhythms coherence among distant regions (15). However, the fact that they don't synapse on excitatory cells together with perforant path inputs suggests that these cells might have different functions than those of dendritic targeting interneurons.

Theta and gamma oscillations have been shown to be important for cognitive processes, especially for circumstances involving active exploration (25). Ketamine, an NMDA blocker known to cause amnesia and other cognitive disorders, was recently shown to cause reduction of theta power in the hippocampus *in vivo*‖, in agreement with the Gillies *et al.* (16) study reporting reduction of theta power by NMDA antagonists *in vitro*. Hajos *et al.* (36) have recently shown that O-LM interneurons possess physiologically important NMDA receptors, which are effectively blocked by ketamine. Although NMDA receptors were not explicitly modeled in our work, their contribution was implicitly accounted for by the external current applied to the O-LM cells. By proposing a central role of the O-LM interneurons for the formation of cell assemblies, our model suggests that ketamine can cause cognitive disorders by lowering the activity of O-LM cells, with consequent loss of theta oscillations and reduction of gamma coordination in the hippocampus.

The main experimental prediction derived from the present work concerns the critical role played by the O-LM interneurons in the ability to form spatially dispersed coherent cell assemblies. *In vivo*, such cell assemblies might consist of cells sparsely arrayed along the longitudinal axis and might not show up in the LFP. *In vitro*, however, with pharmacological models of oscillations, more cells are apt to be involved. We then expect that any intervention lowering the activity of O-LM cells should decrease spatial coherence in the gamma-frequency range. This prediction could be tested by blocking I_h currents or NMDA receptors in these cells. It might also be tested in experimental models of temporal lobe epilepsy, for which a reduction in the number of O-LM cells has been reported (37). The present model network

---

‖Sabolek, H. R., Penley, S. C., Bunce, J. G., Hinman, J. R., Chrobak, J. J. (2006) *Soc Neurosci Abstr* 751.12.

has limitations that should be addressed by future work. Most centrally, phasic input from the dentate and EC to CA3 should be included to investigate the interaction of potentially distinct gamma generators. In simulations with more than one E cell per module, we have not included E–E connections, which are not needed for the formation of gamma rhythms (8); we are treating E–E connections as formed from experience, perhaps as a consequence of gamma synchrony, but not necessary for it. We also note the lack of explicit modeling of important receptors such as NMDA and GABA-B and the fact that the model makes use of just two types of hippocampal interneurons of the many distinct types that have been described (20–22). Nevertheless, the present work already reveals an unintuitive role of the O-LM cells in functionally important coordination of gamma and theta rhythms.

Methods

Anatomical Identification of O-LM Cells. Transverse and longitudinal slices obtained from ventral and whole hippocampus respectively were prepared from C57 mice (P 18–25). Slices with a biocytin-filled interneuron were fixed overnight in 4% paraformaldehyde and processed as described in ref. 38. Subsequently, the cells were reconstructed with the aid of a Neurolucida 3D reconstruction system (MicroBrightField, Williston, VT).

Model Cells and Synapses. To investigate the role of position of synapses along the pyramidal cell dendrites, we used a five-compartment model for the pyramidal cell population (E cell) and single compartment models for the O-LM (O) and basket (I) cells. All simulations were carried out using the NEURON simulation program (39). Detailed information about the model cells and model synapses as well as about numeric and random aspects of this work can be found in *SI Methods* and *SI Appendix*.

Model Networks: Cell Modules and Cell Assemblies. In the present work, we make a distinction between the concepts of cell modules and cell assemblies. A cell module can be regarded as set of cells (E, I, and O) that are located anatomically near each other. The number of E cells in each cell module varied from 1 to 80 cells, whereas the number of each interneuron type (I and O cells) varied from 5 to 50. Both types of interneurons receive phasic excitatory inputs at gamma frequency during the gamma field rhythm (19), suggesting that the pyramidal cell population fires at gamma frequency during gamma field potential, even though each neuron fires only in a small proportion of the cycles (20). This justifies the use of one E cell per module in some simulations, which is intended to model a whole population of synchronous pyramidal cells. We used a greater number of interneurons to have an assessment of their synchronization profiles (especially of the less studied O cells). Cell modules presenting only one E cell are referred to as simple modules. Inside a module, the cells make synaptic connections as schematically shown in Fig. 2*A*. A cell assembly is defined as composed by subsets of modules temporarily displaying phase-locked gamma (note that the cells need not be wired together monosynaptically). Synaptic connections among distinct cell modules were made only through O synapses on E cells (O–E synapses), as schematically shown in Fig. 2*A*.

Model Local Field Potential and Signal Analysis. A "passive" E cell was programmed inside each cell module; it did not send synaptic input to other cells and was made silent by the absence of external drive current. This cell had the same compartments and current distributions as the "active" E cell and received exactly the same synaptic inputs and white noise currents. The model LFP of each compartment of each module consisted of the membrane potential of this passive E cell. The model LFPs were subjected to power spectrum, coherence, and cross-correlation analyses by using standard routines in MATLAB software (see *SI Methods*).

Measures of Gamma Coherence: Phase Histograms and the Phase-Locking Index. The phase differences between two modules were obtained by comparing the time series generated by the spike times of one arbitrary I cell of each module (note that in most of the cases, the I cells are synchronous inside a module). One module is chosen to be the reference gamma rhythm, and the phase of each I cell spike time t_k of the other module is obtained by $phase(t_k) = 2\pi(t_k - t_j)/(t_{j+1} - t_j)$ if $(t_k - t_j) \geq 0$ or $phase(t_k) = 2\pi(t_k - t_j)/(t_j - t_{j-1})$ if $(t_k - t_j) < 0$, where t_j is the closest I spike time in the reference module; $phase(t_k)$ assumes values between $-\pi$ and π. Phase difference histograms were constructed by binning this interval in 25 bins whose centers were separated by a length of $\pi/12$, i.e., $\{-\pi, \ldots, 0, \ldots, \pi\}$. Several simulations with distinct random initial conditions were performed for each parameter set under study (except for Fig. 2), and the final histogram in each case was normalized by the total number of counts. The analysis period was 1 s for each simulation trial.

As a measure of gamma coherence, we used a normalized entropy index for measuring the degree of phase-locking (40) (see *SI Methods*). This phase-locking index (PLI) varies between 0 and 1 (from asynchrony to phase-locking in a single bin).

1. Engel AK, Fries P, Singer W (2001) *Nat Rev Neurosci* 2:704–716.
2. Singer W (1993) *Annu Rev Physiol* 55:349–374.
3. Gray CM (1994) *J Comput Neurosci* 1:11–38.
4. Fries P, Reynolds JH, Rorie AE, Desimone R (2001) *Science* 291:1560–1563.
5. Börgers C, Epstein S, Kopell NJ (2005) *Proc Natl Acad Sci USA* 102:7002–7007.
6. Llinas R, Ribary U, Contreras D, Pedroarena C (1998) *Philos Trans R Soc Lond B* 353:1841–1849.
7. Varela F, Lachaux JP, Rodriguez E, Martinerie J (2001) *Nat Rev Neurosci* 2:229–239.
8. Olufsen MS, Whittington MA, Camperi M, Kopell N (2003) *J Comput Neurosci* 14:33–54.
9. Harris KD, Csicsvari J, Hirase H, Dragoi G, Buzski G (2003) *Nature* 424:552–556.
10. Lisman JE, Idiart MA (1995) *Science* 267:1512–1515.
11. Hasselmo ME, Wyble BP, Wallenstein GV (1996) *Hippocampus* 6:693–708.
12. Kunec S, Hasselmo ME, Kopell N (2005) *J Neurophysiol* 94:70–82.
13. Whittington MA, Traub RD, Jefferys JG (1995) *Nature* 373:612–615.
14. Wang XJ, Buzski G (1996) *J Neurosci* 16:6402–6413.
15. Buzsaki G, Geisler C, Henze DA, Wang XJ (2004) *Trends Neurosci* 27:186–193.
16. Gillies MJ, Traub RD, LeBeau FE, Davies CH, Gloveli T, Buhl EH, Whittington MA (2002) *J Physiol* 543 779–793.
17. Rotstein HG, Pervouchine DD, Acker CD, Gillies MJ, White JA, Buhl EH, Whittington MA, Kopell N (2005) *J Neurophysiol* 94:1509–1518.
18. Gloveli T, Dugladze T, Rotstein H, Traub R, Heinemann U, Monyer H, Whittington M, Kopell N (2005) *Proc Natl Acad Sci USA* 102:13295–13300.
19. Gloveli T, Dugladze T, Saha S, Monyer H, Heinemann U, Traub RD, Whittington MA, Buhl EH (2005) *J Physiol* 562:131–147.
20. Mann EO, Radcliffe CA, Paulsen O (2005) *J Physiol* 562:55–63.
21. Freund TF, Buzski G (1996) *Hippocampus* 6:347–470.
22. Whittington MA, Traub RD (2003) *Trends Neurosci* 26:676–682.
23. Maccaferri G, McBain CJ (1996) *J Physiol* 497 119–130.
24. Maccaferri G, Roberts JD, Szucs P, Cottingham CA, Somogyi P (2000) *J Physiol* 524:91–116.
25. Bragin A, Jando G, Nadasdy Z, Hetke J, Wise K, Buzski G (1995) *J Neurosci* 15:46–60.
26. Penttonen M, Kamondi A, Sik A, Acsdy L, Buzski G (1998) *Eur J Neurosci* 10:718–728.
27. Csicsvari J, Jamieson B, Wise KD, Buzsaki G (2003) *Neuron* 37:311–322.
28. Fisahn A, Pike FG, Buhl EH, Paulsen O (1998) *Nature* 394:186–189.
29. Sik A, Penttonen M, Ylinen A, Buzsaki G (1995) *J Neurosci* 15:6651–6665.
30. Buzsaki G, Buhl DL, Harris KD, Csicsvari J, Czeh B, Morozov A (2003) *Neuroscience* 116:201–211.
31. Bullock TH, Buzsaki G, McClune MC (1990) *Neuroscience* 38:609–619.
32. Ermentrout GB, Kopell N (1998) *Proc Natl Acad Sci USA* 95:1259–1264.
33. Kopell N (1987) in *Neural Control of Rhythmic Movements* (Wiley, New York), pp 369–413.
34. Hoffman DA, Magee JC, Colbert CM, Johnston D (1997) *Nature* 387:869–875.
35. Sik A, Penttonen M, Buzsaki G (1997) *Eur J Neurosci* 9:573–588.
36. Hajos N, Freund TF, Mody I (2002) *Acta Biol Hung* 53:465–472.
37. Cossart R, Dinocourt C, Hirsch JC, Merchan-Perez A, De Felipe J, Ben-Ari Y, Esclapez M, Bernard C (2001) *Nat Neurosci* 4:52–62.
38. Gloveli T, Schmitz D, Empson RM, Dugladze T, Heinemann U (1997) *Neuroscience* 77:629–648.
39. Hines ML, Carnevale NT (1997) *Neural Comput* 9:1179–1209.
40. Hurtado JM, Rubchinsky LL, Sigvardt KA (2004) *J Neurophysiol* 91:1883–1898.

NEUROSCIENCE